Hindawi Publishing Corporation
Boundary Value Problems
Volume 2009, Article ID 568657, 15 pages
doi:10.1155/2009/568657

Research Article

Two-Fluid Mathematical Models for Blood Flow in Stenosed Arteries: A Comparative Study

D. S. Sankar and Ahmad Izani Md. Ismail

School of Mathematical Sciences, University Science Malaysia, 11800 Penang, Malaysia

Correspondence should be addressed to D. S. Sankar, sankar_ds@yahoo.co.in

Received 18 December 2008; Revised 25 January 2009; Accepted 30 January 2009

Recommended by Colin Rogers

The pulsatile flow of blood through stenosed arteries is analyzed by assuming the blood as a two-fluid model with the suspension of all the erythrocytes in the core region as a non-Newtonian fluid and the plasma in the peripheral layer as a Newtonian fluid. The non-Newtonian fluid in the core region of the artery is assumed as a (i) Herschel-Bulkley fluid and (ii) Casson fluid. Perturbation method is used to solve the resulting system of non-linear partial differential equations. Expressions for various flow quantities are obtained for the two-fluid Casson model. Expressions of the flow quantities obtained by Sankar and Lee (2006) for the two-fluid Herschel-Bulkley model are used to get the data for comparison. It is found that the plug flow velocity and velocity distribution of the two-fluid Casson model are considerably higher than those of the two-fluid Herschel-Bulkley model. It is also observed that the pressure drop, plug core radius, wall shear stress and the resistance to flow are significantly very low for the two-fluid Casson model than those of the two-fluid Herschel-Bulkley model. Hence, the two-fluid Casson model would be more useful than the two-fluid Herschel-Bulkley model to analyze the blood flow through stenosed arteries.

Copyright © 2009 D. S. Sankar and A. I. Md. Ismail. This is an open access article distributed under the Creative Commons Attribution License, which permits unrestricted use, distribution, and reproduction in any medium, provided the original work is properly cited.

1. Introduction

There are many evidences that vascular fluid dynamics plays a major role in the development and progression of arterial stenosis. Arteries are narrowed by the development of atherosclerotic plaques that protrude into the lumen, resulting arterial stenosis. When an obstruction developed in an artery, one of the most serious consequences is the increased resistance and the associated reduction of the blood flow to the particular vascular bed supplied by the artery. Thus, the presence of a stenosis leads to the serious circulatory disorder.

Several theoretical and experimental attempts were made to study the blood flow characteristics in the presence of stenosis [1–8]. The assumption of Newtonian behavior of

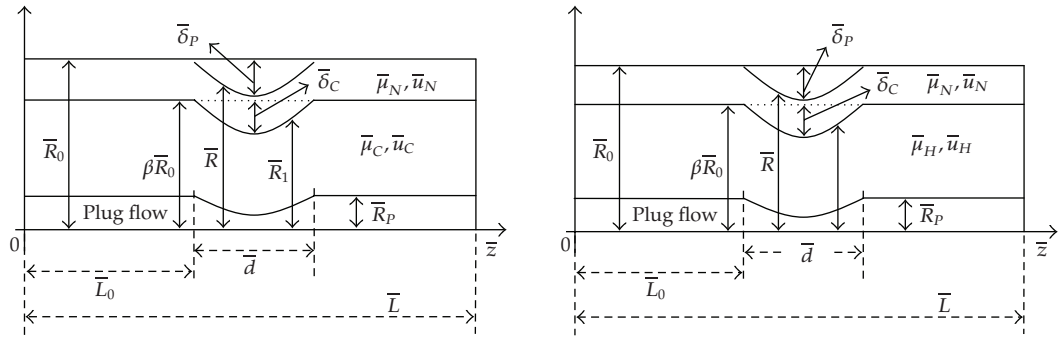

(a) Two-fluid Casson model

(b) Two-fluid H-B model

Figure 1: Geometry of the two-fluid models with arterial stenosis.

blood is acceptable for high shear rate flow through larger arteries [9]. But, blood, being a suspension of cells in plasma, exhibits non-Newtonian behavior at low shear rate ($\dot{\gamma} < 10/\text{sec}$) in small diameter arteries [10]. In diseased state, the actual flow is distinctly pulsatile [11, 12]. Many researchers studied the non-Newtonian behavior and pulsatile flow of blood through stenosed arteries [1, 3, 9, 12].

Bugliarello and Sevilla [13] and Cokelet [14] have shown experimentally that for blood flowing through narrow blood vessels, there a peripheral layer of plasma and a core region of suspension of all the erythrocytes. Thus, for a realistic description of the blood flow, it is appropriate to treat blood as a two-fluid model with the suspension of all the erythrocytes in the core region as a non-Newtonian fluid and plasma in the peripheral region as a Newtonian fluid.

Kapur [15] reported that Casson fluid model and Herschel-Bulkley fluid model are the fluid models with nonzero yield stress and they are more suitable for the studies of the blood flow through narrow arteries. It has been reported by Iida [16] that Casson fluid model is simple to apply for blood flow problems, because of the particular form of its constitutive equation, whereas, Herschel-Bulkley fluid model's constitutive equation is not easy to apply because of the form of its empirical relation, since, it contains one more parameter than the Casson fluid model. It has been demonstrated by Scott-Blair [17] and Copley [18] that the parameters appropriate to Casson fluid—viscosity, yield stress and power law—are adequate for the representation of the simple shear behavior of blood. It has been established by Merrill et al. [19] that Casson fluid model holds satisfactorily for blood flowing in tubes of diameter 130–1300 μm, whereas Herschel-Bulkley fluid model could be used in tubes of diameter 20–100 μm.

Sankar and Lee [20] have developed a two-fluid model for pulsatile blood flow through arterial stenosis treating the fluid in the core region as Herschel-Bulkley fluid. Thus, in this paper, we extend this study to two-fluid Casson model and compare these models and discuss the advantages of the two-fluid Casson model over the two-fluid Herschel-Bulkley (H-B) model.

2. Mathematical Formulation

Consider an axially symmetric, laminar, pulsatile, and fully developed flow of blood (assumed to be incompressible) in the $\overline{z}$ direction through a rigid-walled circular artery with an axially symmetric mild stenosis. The geometry of the arterial stenosis is shown in Figure 1.

We have used the cylindrical polar coordinates $(\overline{r}, \overline{\phi}, \overline{z})$. Blood is represented by a two-fluid model with the suspension of all the erythrocytes in the core region as a non-Newtonian fluid and the plasma in the peripheral region as a Newtonian fluid. The non-Newtonian fluid in the core region is represented by (i) Casson fluid model and (ii) Herschel-Bulkley fluid model. The geometry of the stenosis in the peripheral region (in dimensionless form) and core region are, respectively, given by

$$\overline{R}(z) = \begin{cases} \overline{R}_0 & \text{in the normal artery region,} \\ \overline{R}_0 - \left(\dfrac{\overline{\delta}_P}{2}\right)\left[1+\cos\left(\dfrac{2\pi}{\overline{L}_0}\right)\left\{\overline{z}-\overline{d}-\left(\dfrac{\overline{L}_0}{2}\right)\right\}\right] & \text{in } \overline{d} \le \overline{z} \le \overline{d}+\overline{L}_0, \end{cases} \tag{2.1}$$

$$\overline{R}_1(z) = \begin{cases} \beta\overline{R}_0 & \text{in the normal artery region,} \\ \beta\overline{R}_0 - \left(\dfrac{\overline{\delta}_C}{2}\right)\left[1+\cos\left(\dfrac{2\pi}{\overline{L}_0}\right)\left\{\overline{z}-\overline{d}-\left(\dfrac{\overline{L}_0}{2}\right)\right\}\right] & \text{in } \overline{d} \le \overline{z} \le \overline{d}+\overline{L}_0, \end{cases} \tag{2.2}$$

where $\overline{R}(\overline{z})$ and $\overline{R}_1$ are the radii of the stenosed artery with the peripheral region and core region, respectively; $\overline{R}_0$ and $\beta\overline{R}_0$ are the radii of the normal artery and core region of the normal artery, respectively; β is the ratio of the central core radius to the normal artery radius; $\overline{L}_0$ is the length of the stenosis; $\overline{d}$ indicates the location of the stenosis; $\overline{\delta}_P$ and $\overline{\delta}_C$ are the maximum projections of the stenosis in the peripheral region and core region, respectively, such that $[\overline{\delta}_P/\overline{R}_0] \ll 1$ and $[\overline{\delta}_C/\overline{R}_0] \ll 1$.

2.1. Two-Fluid Casson Model

2.1.1. Governing Equations

It can be shown that the radial velocity is negligibly small and can be neglected for a low Reynolds number flow. The basic momentum equations governing the flow are

$$\begin{aligned} \overline{\rho}_C\left(\frac{\partial\overline{u}_C}{\partial\overline{t}}\right) &= -\left(\frac{\partial\overline{p}}{\partial\overline{z}}\right) - \left(\frac{1}{\overline{r}}\right)\left(\frac{\partial\left(\overline{r}\overline{\tau}_C\right)}{\partial\overline{r}}\right) \quad \text{in } 0 \le \overline{r} \le \overline{R}_1(\overline{z}), \\ \overline{\rho}_N\left(\frac{\partial\overline{u}_N}{\partial\overline{t}}\right) &= -\left(\frac{\partial\overline{p}}{\partial\overline{z}}\right) - \left(\frac{1}{\overline{r}}\right)\left(\frac{\partial\left(\overline{r}\overline{\tau}_N\right)}{\partial\overline{r}}\right) \quad \text{in } \overline{R}_1(\overline{z}) \le \overline{r} \le \overline{R}(\overline{z}), \end{aligned} \tag{2.3}$$

where the shear stress $\overline{\tau} = |\overline{\tau}_{\overline{r}\overline{z}}| = -\overline{\tau}_{\overline{r}\overline{z}}$ (since $\overline{\tau} = \overline{\tau}_C$ or $\overline{\tau} = \overline{\tau}_N$); $\overline{p}$ is the pressure; $\overline{u}_C$ and $\overline{u}_N$ are the axial velocities of the fluid in the core region and peripheral region, respectively; $\overline{\tau}_C$ and $\overline{\tau}_N$ are the shear stresses of the Casson fluid and Newtonian fluid, respectively; $\overline{\rho}_C$ and $\overline{\rho}_N$ are the densities of the Casson fluid and Newtonian fluid, respectively; $\overline{t}$ is the time. The relationships between the shear stress and strain rate of the fluids in motion in the

core region (Casson fluid) and peripheral region (Newtonian fluid) are given by

$$\sqrt{\overline{\tau}_C} = \sqrt{-\overline{\mu}_C\left(\frac{\partial \overline{u}_C}{\partial \overline{r}}\right)} + \sqrt{\overline{\tau}_y} \quad \text{if } \overline{\tau}_C \geq \overline{\tau}_y,\ \overline{R}_p \leq \overline{r} \leq \overline{R}_1(\overline{z}), \tag{2.4}$$

$$\left(\frac{\partial \overline{u}_C}{\partial \overline{r}}\right) = 0 \quad \text{if } \overline{\tau}_C \leq \overline{\tau}_y,\ 0 \leq \overline{r} \leq \overline{R}_p, \tag{2.5}$$

$$\overline{\tau}_N = -\overline{\mu}_N\left(\frac{\partial \overline{u}_N}{\partial \overline{r}}\right) \quad \text{if } \overline{R}_1(\overline{z}) \leq \overline{r} \leq \overline{R}(\overline{z}), \tag{2.6}$$

where $\overline{\mu}_C$ and $\overline{\mu}_N$ are the viscosities of the Casson and Newtonian fluids, respectively; $\overline{\tau}_y$ is the yield stress; $\overline{R}_P$ is the plug core radius. The boundary conditions are

$$\begin{gathered} \overline{\tau}_C \text{ is finite and } \frac{\partial \overline{u}_C}{\partial \overline{r}} = 0 \quad \text{at } \overline{r} = 0, \\ \overline{u}_N = 0 \quad \text{at } r = \overline{R}, \\ \overline{\tau}_C = \overline{\tau}_N, \quad \overline{u}_C = \overline{u}_N \quad \text{at } \overline{r} = \overline{R}_1. \end{gathered} \tag{2.7}$$

Since the pressure gradient is a function of $\overline{z}$ and $\overline{t}$, we assume

$$-\left(\frac{\partial \overline{p}}{\partial \overline{z}}\right) = \overline{q}(\overline{z}) f(\overline{t}), \tag{2.8}$$

where $\overline{q}(\overline{z}) = -(\partial \overline{p}/\partial \overline{z})(\overline{z}, 0)$. Since any periodic function can be expanded in a Fourier sine series, it is reasonable to choose $1 + A \sin \overline{\omega}\overline{t}$ as a good approximation for $f(\overline{t})$,where A and $\overline{\omega}$ are the amplitude and angular frequency of the flow, respectively. We introduce the following nondimensional variables:

$$\begin{gathered} z = \frac{\overline{z}}{\overline{R}_0}, \qquad R(z) = \frac{\overline{R}(\overline{z})}{\overline{R}_0}, \qquad R_1(z) = \frac{\overline{R}_1(\overline{z})}{\overline{R}_0}, \qquad r = \frac{\overline{r}}{\overline{R}_0}, \qquad d = \frac{\overline{d}}{\overline{R}_0}, \qquad L_0 = \frac{\overline{L}_0}{\overline{R}_0}, \\ q(z) = \frac{\overline{q}(\overline{z})}{\overline{q}_0}, \qquad \varepsilon_C = \alpha_C^2 = \frac{\overline{R}_0^2 \overline{\omega} \overline{\rho}_C}{\overline{\mu}_C}, \qquad \varepsilon_N = \alpha_N^2 = \frac{\overline{R}_0^2 \overline{\omega} \overline{\rho}_N}{\overline{\mu}_N}, \qquad R_P = \frac{\overline{R}_P}{\overline{R}_0}, \\ \delta_P = \frac{\overline{\delta}_P}{\overline{R}_0}, \qquad \delta_C = \frac{\overline{\delta}_C}{\overline{R}_0}, \qquad u_C = \frac{\overline{u}_C}{\overline{q}_0 \overline{R}_0^2/4\overline{\mu}_C}, \qquad u_N = \frac{\overline{u}_N}{\overline{q}_0 \overline{R}_0^2/4\overline{\mu}_N}, \\ \tau_C = \frac{\overline{\tau}_C}{\overline{q}_0 \overline{R}_0/2}, \qquad \tau_N = \frac{\overline{\tau}_N}{\overline{q}_0 \overline{R}_0/2}, \qquad \theta = \frac{\overline{\tau}_y}{\overline{q}_0 \overline{R}_0/2}, \qquad t = \overline{\omega}\overline{t}, \end{gathered} \tag{2.9}$$

where $\overline{q}_0$ is the negative of the pressure gradient in the normal artery; α_C and α_N are the pulsatile Reynolds numbers of the Casson fluid and Newtonian fluid, respectively. Using the

nondimensional variables, (2.1)–(2.4) are simplified to

$$\varepsilon_C\left(\frac{\partial u_C}{\partial t}\right) = 4q(z)f(t) - \frac{(2/r)\partial(r\tau_C)}{\partial r} \quad \text{if } 0 \le r \le R_1(z), \tag{2.10}$$

$$\sqrt{\tau_C} = \sqrt{\frac{(-1/2)\partial u_C}{\partial r}} + \sqrt{\theta} \quad \text{if } \tau_C \ge \theta,\ R_p \le r \le R_1(z), \tag{2.11}$$

$$\frac{\partial u_C}{\partial r} = 0 \quad \text{if } \tau_C \le \theta,\ 0 \le r \le R_p, \tag{2.12}$$

$$\begin{aligned} \frac{\varepsilon_N \partial u_N}{\partial t} &= 4q(z)f(t) - \frac{(2/r)\partial(r\tau_N)}{\partial r}, \\ \tau_N &= -\left(\frac{1}{2}\right)\left(\frac{\partial u_N}{\partial r}\right), \end{aligned} \qquad \text{if } R_1(z) \le r \le R(z), \tag{2.13}$$

where

$$f(t) = 1 + A\sin t. \tag{2.14}$$

The boundary conditions (in the dimensionless form) are

$$\begin{gathered} \tau_C \text{ is finite and } \frac{\partial u_C}{\partial r} = 0 \quad \text{at } r = 0, \\ \tau_C = \tau_N, \quad u_C = u_N \quad \text{at } r = R_1, \\ u_N = 0 \quad \text{at } r = R. \end{gathered} \tag{2.15}$$

The geometry of the stenosis in the peripheral region and core region (in the dimensionless form) are given by

$$\begin{aligned} R(z) &= \begin{cases} 1 & \text{in the normal artery region,} \\ 1 - \left(\dfrac{\delta_P}{2}\right)\left\{1 + \cos\left[\left(\dfrac{2\pi}{L_0}\right)\left(z - d - \left(\dfrac{L_0}{2}\right)\right)\right]\right\} & \text{in } d \le z \le d + L_0, \end{cases} \\ R_1(z) &= \begin{cases} \beta & \text{in the normal artery region,} \\ \beta - \left(\dfrac{\delta_C}{2}\right)\left\{1 + \cos\left[\left(\dfrac{2\pi}{L_0}\right)\left(z - d - \left(\dfrac{L_0}{2}\right)\right)\right]\right\} & \text{in } \ d \le z \le d + L_0. \end{cases} \end{aligned} \tag{2.16}$$

The nondimensional volume flow rate Q is given by

$$Q = 4\int_0^{R(z)} u(r,z,t)\ r\,dr, \tag{2.17}$$

where $Q = \overline{Q}/(\pi\overline{R}_0^4\overline{q}_0/8\overline{\mu}_0)$; $\overline{Q}$ is the volume flow rate.

2.1.2. Method of Solution

When we nondimensionalize the constitutive (2.1), (2.2), ε_C and ε_N occur naturally and these are time dependent and hence, it is more appropriate to expand (2.10)–(2.13) about ε_C and ε_N. Let us expand the plug core velocity u_p and the velocity in the core region u_C in the perturbation series of ε_C as follows: (where $\varepsilon_C \ll 1$)

$$\begin{aligned} u_p(z,t) &= u_{0p}(z,t) + \varepsilon_C\, u_{1p}(z,t) + \cdots, \\ u_C(r,z,t) &= u_{0C}(r,z,t) + \varepsilon_C u_{1C}(r,z,t) + \cdots. \end{aligned} \tag{2.18}$$

Similarly, one can expand u_N, τ_P, τ_C, τ_N, and R_P in powers of ε_C and ε_N, where $\varepsilon_N \ll 1$. Using the perturbation series in (2.10), (2.11) and then equating the constant terms and ε_C terms, the differential equations of the core region become

$$\begin{aligned} \frac{\partial(r\tau_{0C})}{\partial r} &= 2q(z)f(t)r, \qquad \frac{\partial u_{0C}}{\partial t} = -\frac{(2/r)\partial(r\tau_{1C})}{\partial r}, \\ -\frac{\partial u_{0C}}{\partial r} &= 2\left(\tau_{0C} - 2\sqrt{\theta\tau_{0C}} + \theta\right), \qquad -\frac{\partial u_{1C}}{\partial r} = 2\tau_{1C}\left(1 - \sqrt{\frac{\theta}{\tau_{0C}}}\right). \end{aligned} \tag{2.19}$$

Similarly, using the perturbation series expansions in (2.13) and then equating the constant terms and ε_N terms, the differential equations of the peripheral region become

$$\begin{aligned} \frac{\partial(r\tau_{0N})}{\partial r} &= 2q(z)f(t)r, \qquad \frac{\partial u_{0N}}{\partial t} = -\frac{(2/r)\partial(r\tau_{1N})}{\partial r}, \\ -\frac{\partial u_{0N}}{\partial r} &= 2\tau_{0N}, \qquad -\frac{\partial u_{1N}}{\partial r} = 2\tau_{1N}. \end{aligned} \tag{2.20}$$

Substituting the perturbation series expansions in (2.15) and then equating the constant terms and ε_C and ε_N terms, we get

$$\begin{aligned} &\tau_{0p} \text{ and } \tau_{1p} \text{ are finite and } \frac{\partial u_{0P}}{\partial r} = 0, \qquad \frac{\partial u_{1P}}{\partial r} = 0 \quad \text{at } r = 0, \\ &\tau_{0C} = \tau_{0N}, \quad \tau_{1C} = \tau_{1N}, \quad u_{0C} = u_{0N}, \quad u_{1C} = u_{1N} \quad \text{at } r = R_1, \\ &u_{0N} = u_{1N} = 0 \quad \text{at } r = R. \end{aligned} \tag{2.21}$$

Solving the system of (2.19) and (2.20) using (2.21) for the unknowns u_{0C}, u_{1C}, τ_{0C}, τ_{1C}, u_{0N}, u_{1N}, τ_{0N}, and τ_{1N}, one can obtain

$$\tau_{0p} = \psi R_{0p}, \qquad \tau_{0C} = \psi r, \qquad \tau_{0N} = \psi r, \tag{2.22}$$

$$u_{0N} = \psi R^2\left(1 - \xi^2\right), \tag{2.23}$$

$$u_{0C} = \psi R^2\left\{\left(1 - \Omega^2\right) + \Omega^2\left[\left(1 - \xi_1^2\right) - \left(\frac{8}{3}\right)\sigma_1^{1/2}\left(1 - \sigma_1^{3/2}\right) + 2\sigma_1\left(1 - \xi_1\right)\right]\right\}, \tag{2.24}$$

$$u_{0P} = \psi R^2 \left\{ (1-\Omega^2) + \Omega^2 \left[(1-\chi^2) - \left(\frac{8}{3}\right)\sigma_1^{1/2}(1-\chi^{3/2}) + 2\sigma_1(1-\chi) \right] \right\}, \tag{2.25}$$

$$\tau_{1p} = -\psi BR^3 \left\{ \left(\frac{1}{4}\right)\sigma(1-\Omega^2) + \Omega^3\sigma_1 \left[\left(\frac{1}{4}\right) - \left(\frac{1}{3}\right)\sigma_1^{1/2} + \left(\frac{1}{12}\right)\sigma_1^2 \right] \right\}, \tag{2.26}$$

$$\tau_{1C} = -\psi BR^3 \left\{ \left(\frac{1}{4}\right)\xi(1-\Omega^2) - \left(\frac{1}{8}\right)\Omega^3 \left[2\xi_1 - \xi_1^3 - \sigma_1^4\xi_1^{-1} - \left(\frac{8}{21}\right)\sigma_1^{1/2}(7\xi_1 - 4\xi_1^{5/2} - 3\sigma_1^{7/2}\xi_1^{-1}) \right] \right\}, \tag{2.27}$$

$$\tau_{1N} = -\psi BR^2 R_1 \left\{ \left[\left(\frac{1}{4}\right)\xi_1 - \left(\frac{1}{8}\right)\Omega^2\xi_1^{-1} - \left(\frac{1}{8}\right)\Omega^2\xi_1^3 \right] + \xi_1^{-1}\Omega^2 \left[\left(\frac{1}{8}\right) - \left(\frac{1}{7}\right)\sigma_1^{1/2} + \left(\frac{1}{56}\right)\sigma_1^4 \right] \right\}, \tag{2.28}$$

$$\begin{aligned} u_{1N} = -\psi BR^3 R_1 \Bigg\{ & \left[\left(\frac{1}{4}\right)\Omega^{-1}(1-\xi^2) - \left(\frac{1}{4}\right)\Omega^3 \log\xi^{-1} - \left(\frac{1}{16}\right)\Omega^{-1}(1-\xi^4) \right] \\ & - \Omega^3 \log\xi \left[\left(\frac{1}{4}\right) - \left(\frac{2}{7}\right)\sigma_1^{1/2} + \left(\frac{1}{28}\right)\sigma_1^4 \right] \Bigg\}, \end{aligned} \tag{2.29}$$

$$\begin{aligned} u_{1C} = -\psi BR^3 R_1 \Bigg\{ & \left[\left(\frac{3}{16}\right)\Omega^{-1} - \left(\frac{1}{4}\right)\Omega + \left(\frac{1}{16}\right)\Omega^3 + \left(\frac{1}{4}\right)\Omega^3 \log\Omega \right] \\ & - \Omega^3 \log\Omega \left[\left(\frac{1}{4}\right) - \left(\frac{2}{7}\right)\sigma_1^{1/2} + \left(\frac{1}{28}\right)\sigma_1^4 \right] \\ & + \Omega(1-\Omega^2) \left[\left(\frac{1}{4}\right)(1-\xi_1^2) - \left(\frac{1}{3}\right)\sigma_1^{1/2}(1-\xi_1^{3/2}) \right] \\ & + \Omega^3 \left[\left(\frac{1}{4}\right)(1-\xi_1^2) - \left(\frac{1}{3}\right)\sigma_1^{1/2}(1-\xi_1^{3/2}) - \left(\frac{1}{16}\right)(1-\xi_1^4) \right. \\ & \quad + \left(\frac{53}{294}\right)\sigma_1^{1/2}(1-\xi_1^{7/2}) - \left(\frac{1}{3}\right)(1-\xi_1^2) + \left(\frac{4}{9}\right)\sigma_1(1-\xi_1^{3/2}) \\ & \quad \left. - \left(\frac{8}{63}\right)\sigma_1(1-\xi_1^3) - \left(\frac{1}{28}\right)\sigma_1^4 \log\xi_1 + \left(\frac{1}{14}\right)\sigma_1^{9/2}(1-\xi_1^{-1/2}) \right] \Bigg\}, \end{aligned} \tag{2.30}$$

$$\begin{aligned} u_{1P} = -\psi BR^3 R_1 \Bigg\{ & \left(\left(\frac{3}{16}\right)\Omega^{-1} - \left(\frac{1}{4}\right)\Omega + \left(\frac{1}{16}\right)\Omega^3 + \left(\frac{1}{4}\right)\Omega^3 \log\Omega \right) \\ & - \Omega^3 \log\Omega \left(\left(\frac{1}{4}\right) - \left(\frac{2}{7}\right)\sigma_1^{1/2} + \left(\frac{1}{28}\right)\sigma_1^4 \right) \\ & + \Omega(1-\Omega^2) \left[\left(\frac{1}{4}\right)(1-\sigma_1^2) - \left(\frac{1}{3}\right)\sigma_1^{1/2}(1-\sigma_1^{3/2}) \right] \\ & + \Omega^3 \left[\left(\frac{1}{4}\right)(1-\sigma_1^2) - \left(\frac{1}{3}\right)\sigma_1^{1/2}(1-\sigma_1^{3/2}) - \left(\frac{1}{16}\right)(1-\sigma_1^4) \right. \\ & \quad - \left(\frac{53}{294}\right)\sigma_1^{1/2}(1-\sigma_1^{7/2}) - \left(\frac{1}{3}\right)(1-\sigma_1^2) + \left(\frac{4}{9}\right)\sigma_1(1-\sigma_1^{3/2}) \\ & \quad \left. + \left(\frac{8}{63}\right)2\sigma_1(1-\sigma_1^3) - \left(\frac{1}{28}\right)\sigma_1^4 \log\sigma_1 + \left(\frac{1}{14}\right)\sigma_1^{9/2}(1-\sigma_1^{-1/2}) \right] \Bigg\}, \end{aligned} \tag{2.31}$$

where $\psi = q(z)f(t), k^2 = r|_{r_{0p=\theta}} = R_{0p} = \theta/[q(z)f(t)], B = [1/f(t)](df(t)/dt), \xi = r/R, \xi_1 = r/R_1, \Omega = R_1/R, \sigma = k^2/R, \sigma = k^2/R_1$, and $\chi = R_{0p}/R_1$. The wall shear stress τ_w can be obtained as follows:

$$\begin{aligned}\tau_w &= \left(\tau_{0N} + \varepsilon_N \tau_{1N}\right)_{r=R} = \tau_{0w} + \varepsilon_N \tau_{1w} \\ &= \psi\left\{R - \left(\frac{1}{8}\right)BR^3\varepsilon_N(1-\Omega^4) - \left(\frac{1}{8}\right)BR_1^3\varepsilon_N\Omega\left[1 - \left(\frac{8}{7}\right)\sigma_1^{1/2} + \left(\frac{1}{7}\right)\sigma_1^4\right]\right\}.\end{aligned} \tag{2.32}$$

Using (2.23)–(2.25) and (2.29)–(2.31) in (2.17), the volume flow rate is obtained as

$$\begin{aligned}Q = \psi R^4\Bigg\{&(1-\Omega^2)(1+3\Omega^2) + \Omega^4\left[1 - \left(\frac{16}{7}\right)\sigma_1^{1/2} + \left(\frac{4}{3}\right)\sigma_1 - \left(\frac{1}{21}\right)\sigma_1^4\right]\Bigg\} \\ &- \varepsilon_C \nabla B R^3 R_1^3\Bigg\{\left[\left(\frac{3}{8}\right)\Omega^{-1} - \left(\frac{1}{2}\right)\Omega + \left(\frac{1}{8}\right)\Omega^3 + \left(\frac{1}{2}\right)\Omega^3\log\Omega\right] \\ &\quad - \Omega^3\log\Omega\left[\left(\frac{1}{2}\right) - \left(\frac{4}{7}\right)\sigma_1^{1/2} + \left(\frac{1}{14}\right)\sigma_1^4\right] \\ &\quad + \Omega(1-\Omega^2)\left[\left(\frac{1}{4}\right) - \left(\frac{2}{7}\right)\sigma_1^{1/2} + \left(\frac{1}{28}\right)\sigma_1^4\right] \\ &\quad + \Omega^3\Bigg[\left(\frac{1}{6}\right) - \left(\frac{30}{77}\right)\sigma_1^{1/2} + \left(\frac{8}{35}\right)\sigma_1 - \left(\frac{1}{3}\right)\sigma_1^{5/2} + \left(\frac{1}{14}\right)\sigma_1^4 \\ &\qquad + \left(\frac{5}{21}\right)\sigma_1^{9/2} - \left(\frac{41}{770}\right)\sigma_1^6 - \left(\frac{1}{14}\right)\sigma_1^6\log\sigma_1 + \left(\frac{1}{14}\right)\sigma_1^4(1-\sigma_1^2)\log k\Bigg]\Bigg\} \\ &- \varepsilon_N \psi B R^5 R_1\Bigg\{\left[\left(\frac{1}{6}\right)\Omega^{-1} - \left(\frac{3}{8}\right)\Omega + \left(\frac{5}{24}\right)\Omega^5 - \left(\frac{1}{2}\right)\Omega^3(1-\Omega^2)\log R_1\right] \\ &\quad + \Omega^4(1-\Omega^2)(1+2\log R_1)\left[\left(\frac{1}{4}\right) - \left(\frac{2}{7}\right)\sigma_1^{1/2} + \left(\frac{1}{28}\right)\sigma_1^4\right]\Bigg\}.\end{aligned} \tag{2.33}$$

The shear stress $\tau_C = \tau_{0C} + \varepsilon_H \tau_{1C}$ at $r = R_p$ is given by

$$\left|\tau_{0C} + \varepsilon_C \tau_{1C}\right|_{r=R_p} = \theta. \tag{2.34}$$

Using Taylor's series of τ_{0C} and τ_{1C} about R_{0p} and using $\tau_{0C}|_{r=R_{0p}} = \theta$, we get

$$R_{1p} = \frac{-\tau_{1C}\,|_{r=R_{0p}}}{\psi}. \tag{2.35}$$

Using (2.22), (2.27), and (2.35) in the two term approximated perturbation series of R_P, the expression for R_P can be obtained as

$$R_p = k^2 - \left(\frac{1}{4}\right)B\varepsilon_C R^3\left[\sigma^2(1-\Omega^2) + \Omega^3\left(\sigma_1 - \frac{4\sigma_1^{3/2}}{3} + \frac{\sigma_1^3}{3}\right)\right]. \tag{2.36}$$

The resistance to flow is given by

$$\Lambda = \frac{[\Delta p\, f(t)]}{Q}, \tag{2.37}$$

where Δp is the pressure drop. When $R_1 = R$, the present model reduces to the single fluid Casson model and in such case, the expressions obtained in the present model for velocity u_C, shear stress τ_C, wall shear stress τ_w, flow rate Q and plug core radius R_p are in good agreement with those of Chaturani and Samy [12].

2.2. *Two-Fluid Herschel-Bulkley Model*

The basic momentum equations governing the flow and the constitutive equations in the nondimensional form are

$$\varepsilon_H\left(\frac{\partial u_H}{\partial t}\right) = 4q(z)f(t) - \left(\frac{2}{r}\right)\left(\frac{\partial(r\tau_H)}{\partial r}\right) \quad \text{if } 0 \le r \le R_1(z), \tag{2.38}$$

$$\varepsilon_H\left(\frac{\partial u_N}{\partial t}\right) = 4q(z)f(t) - \left(\frac{2}{r}\right)\left(\frac{\partial(r\tau_N)}{\partial r}\right) \quad \text{if } R_1(z) \le r \le R(z), \tag{2.39}$$

$$\tau_H = \sqrt[n]{-\left(\frac{1}{2}\right)\left(\frac{\partial u_H}{\partial r}\right)} + \theta \quad \text{if } \tau_H \ge \theta,\ R_p \le r \le R_1(z), \tag{2.40}$$

$$\frac{\partial u_H}{\partial r} = 0 \quad \text{if } \tau_H \le \theta,\ 0 \le r \le R_p, \tag{2.41}$$

$$\tau_N = -\left(\frac{1}{2}\right)\left(\frac{\partial u_N}{\partial r}\right) \quad \text{if } R_1(z) \le r \le R(z). \tag{2.42}$$

The boundary conditions (in dimensionless form) of this model are similar to the boundary conditions of the two-fluid Casson model given in (2.7). Equations (2.38)–(2.42) are also solved using perturbation method with the help of the appropriate boundary conditions as in the case of the two-fluid Casson model. The details of the derivation of the expressions for shear stress, velocity, flow rate, plug core radius, wall shear stress and resistance to flow are given in Sankar and Lee [20].

3. Results and Discussion

The objective of the present analysis is to compare and bring out the advantages of the two-fluid Casson model over the two-fluid Herschel-Bulkley model. It is observed that the typical value of the power law index n for blood flow models is taken as 0.95 [3]. The value 0.1 is used for the nondimensional yield stress θ in this study. Even though the range of the amplitude A is from 0 to 1, we have used the value 0.5. The value 0.5 is used for the pulsatile Reynolds numbers $\alpha_{\mathrm{H}}, \alpha_{\mathrm{C}}$ and pulsatile Reynolds number ratio α of both the two-fluid models [11]. The value of the ratio β of central core radius $\beta\overline{R}_0$ to the normal artery radius $\overline{R}_0$ in the unobstructed artery is generally taken as 0.95 [15]. Following Shukla et al. [21], relations $R_1 = \beta R$ and $\delta_c = \beta\delta_p$ are used to estimate R_1 and δ_c. The maximum thickness of the stenosis

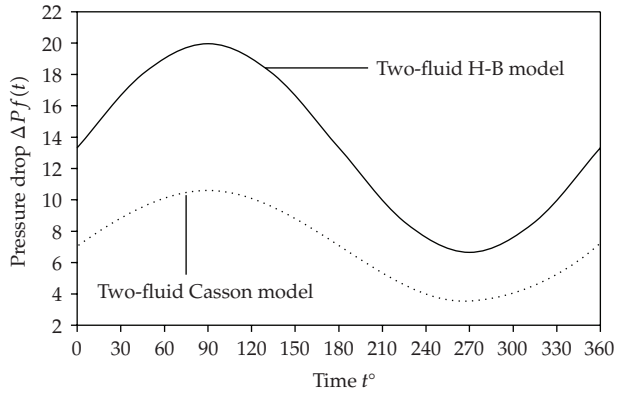

Figure 2: Variation of pressure drop in a time cycle of the two-fluid Casson and H-B models.

in the peripheral region δ_P is taken as 0.1 [11]. The steady flow rate Q_S value is taken as 1.0 [12]. It is observed that in the expression of the flow rate of the two-fluid Casson model, $f(t)$, R and θ are the knowns, and Q and $q(z)$ are the unknowns to be determined. A careful analysis of the flow rate expression reveals the fact that $q(z)$ is the pressure gradient of the steady flow. Thus, if steady flow is assumed, then the expression of the flow rate can be solved for $q(z)$ [3, 12]. For steady flow, the expression for flow rate of the two-fluid Casson model reduces to

$$(R^4-4R^2R_1^2+3R_1^4)y^4+\left[(R_1y)^4-\left(\frac{16}{7}\right)\sqrt{\theta}\left(\sqrt{R_1y}\right)^7+\left(\frac{4}{3}\right)\theta(R_1y)^3-\left(\frac{1}{21}\right)\theta^4\right]-Q_Sy^3=0. \tag{3.1}$$

The similar equation of the two-fluid Herschel-Bulkley model is

$$\begin{aligned}&(R^2-R_1^2)\left[4\left(\frac{\theta}{\Omega}\right)^2+(R^2-R_1^2)\right]y^3+\left[\frac{4}{(n+2)(n+3)}\right],\\&\left\{(n+2)(R_1y)^{n+3}-n(n+3)\theta(R_1y)^{n+2}+(n^2+2n-2)\theta^{n+2}\right\}-Q_Sy^3=0.\end{aligned} \tag{3.2}$$

The variation of pressure drop in a time cycle of the two-fluid Herschel-Bulkley (H-B) and Casson models with $\theta=\delta_P=0.1$, A = 0.5, and $\beta=0.95$ is shown in Figure 2. It is observed that for both the two-fluid models the pressure drop increases as time t (in degrees) increases from 0° to 90°, then it decreases as t increases from 90° to 270°, and again the pressure drop increases as t increases further from 270° to 360°. The pressure drop is maximum at 90° and minimum at 270°. It is found that, at any time, the pressure drop of the two-fluid Casson model is considerably much lower than that of the two-fluid H-B model while all the other parameters held constant. Figure 3 depicts the variation of the plug core radius with axial distance of the two-fluid H-B and Casson models with $\theta=\delta_P=0.1$, A = 0.5, and $\beta=0.95$. It is noticed that the plug core radius decreases as the axial variable z increases from 4 to 5 and it increases symmetrically when the axial variable increases from 5 to 6. It is noted that for a given set of values of the parameters, the plug core radius values of the two-fluid Casson model are significantly much lower than that of the two-fluid H-B model.

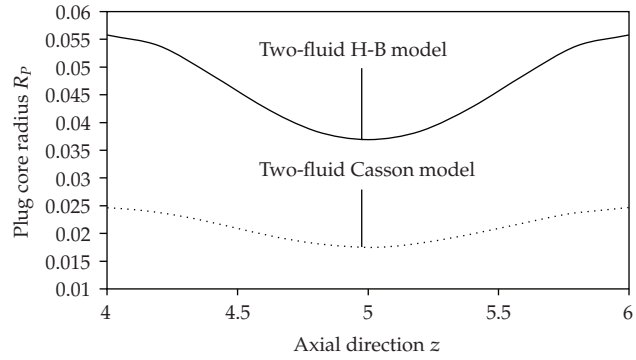

Figure 3: Variation of plug core radius with axial distance of the two-fluid Casson and Herschel-Bulkley models.

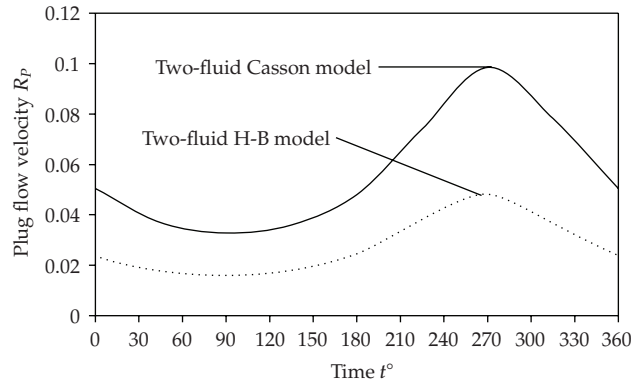

Figure 4: Variation of plug flow velocity in a time cycle of the two-fluid Casson and two fluid Herschel-Bulkley models.

3.1. Plug Flow Velocity

The variation of the plug flow velocity in a time cycle of the two-fluid Casson and H-B models with $\theta = \delta_P = 0.1$, A $= 0.5, \alpha = \alpha_H = \alpha_C = 0.5, \alpha_N = 0.25$, $\beta = 0.95$, and $z = 5$ is depicted in Figure 4. It is seen that the plug flow velocity decreases as time t (in degrees) increases from 0° to 90°, then it increases as t increases from 90° to 270°, and then again it decreases from 270° to 360°. The plug flow velocity is minimum at 90° and maximum at 270°. It is noted that the plug flow velocity of the two-fluid Casson model is considerably higher than that of the two-fluid H-B model.

3.2. Wall Shear Stress

Figure 5 shows the variation of the wall shear stress in a time cycle of the two-fluid Casson and H-B models with $\theta = \delta_P = 0.1$, A $= 0.5, \alpha = \alpha_H = \alpha_C = 0.5, \alpha_N = 0.25, \beta = 0.95$, and $z = 5$. The behavior of the wall shear stress is just reversed of the two-fluid models, that we observed in Figure 4 for the plug flow velocity.

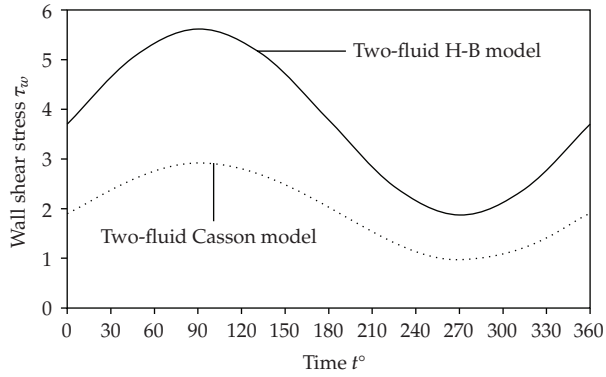

Figure 5: Variation of wall shear stress in a cycle of the two-fluid Casson and two fluid Herschel-Bulkley models.

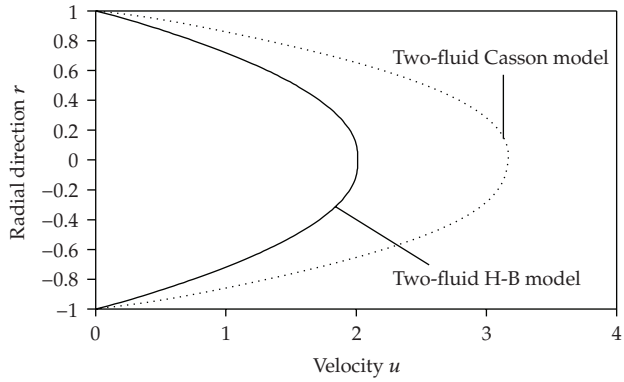

Figure 6: Velocity distribution of the two-fluid Casson and two-fluid Herschel-Bulkley model.

3.3. Velocity Distribution

The velocity distributions of the two-fluid H-B and Casson models with $\theta = \delta_P = 0.1$, A = 0.5, $\alpha = \alpha_H = \alpha_C = 0.5, \alpha_N = 0.25, \beta = 0.95$, and $t = 45°$ are sketched in Figure 6. One can notice the plug flow around the tube axis for both the fluid models. It is further recorded that, for a given set values of the parameters, a significantly high-magnitude velocity profile is found in the two-fluid Casson model than in the two-fluid H-B model.

3.4. Resistance to Flow

The variation of resistance to flow with peripheral layer stenosis height of the two-fluid Casson and H-B models with $\theta = \delta_P = 0.1$, A = 0.5, $\alpha = \alpha_H = \alpha_C = 0.5, \alpha_N = 0.25, \beta = 0.95$, and $t = 45°$ is shown in Figure 7. It is observed that the resistance to flow increases nonlinearly with the increase of the peripheral stenosis height. It is of interest to note that, for any value of the stenosis height, the resistance to flow of the two-fluid Casson model is considerably much lower than that of the H-B model.

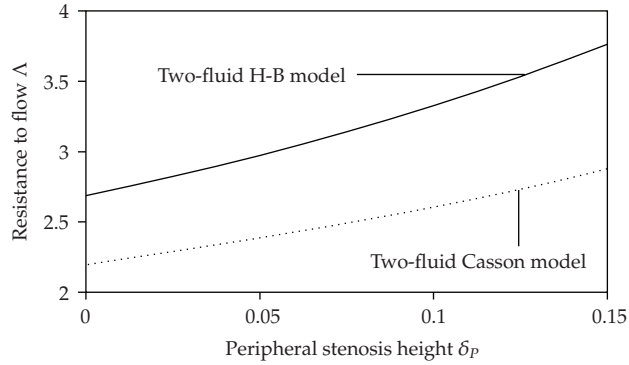

Figure 7: Variation of resistance to flow with peripheral layer stenosis height of the two-fluid Casson and two-fluid Herschel-Bulkley models.

Table 1: Estimates of the wall shear stress (τ_w) and percentage of increase in the wall shear stress (τ_w) of the two-fluid Casson model and two-fluid Herschel-Bulkley model over uniform diameter tube for different stenosis sizes with $A = \alpha = \alpha_H = 0.5$, $\beta = 0.985$, $\theta = 0.1$, and $t = 45^\circ$.

Stenosis height δ_p	Estimates of the wall shear stress		Estimates of the percentage of increase in wall shear stress	
	Two-fluid Casson model	Two-fluid H-B model with $n = 0.95$	Two-fluid Casson model	Two-fluid H-B model with $n = 0.95$
0.025	1.677	3.0057	5.45	7.43
0.050	1.8058	3.1852	11.42	15.70
0.075	1.9495	3.3826	17.99	24.93
0.100	2.1102	3.6005	25.24	35.25
0.125	2.2907	3.8416	33.26	46.84
0.150	2.4939	4.1093	42.16	59.89

3.5. Quantification of the Wall Shear Stress and Resistance to Flow

The wall shear stress (τ_w) and resistance to flow (Λ) are physiologically important quantities which play an important role in the formation of platelets [22]. High wall shear stress not only damages the vessel wall and causes intimal thickening but also activates platelets, causes platelet aggregation, and finally results in the formation of thrombus [6]. Estimates of the wall shear stress (τ_w) and the percentage of increase in the wall shear stress of the two-fluid Casson model and two-fluid Herschel-Bulkley model with $n = 0.95$ for different stenosis heights with $\beta = 0.985$, $A = \alpha = \alpha_H = 0.5$, $\theta = 0.1$ and $t = 45^\circ$ are computed in Table 1. It is found that for the range 0.025–0.15 of the stenosis height, the corresponding range of the percentage of increase in the estimates of the wall shear stress of the two-fluid Casson model and two-fluid Herschel-Bulkley model with $n = 0.95$ are 5.45–42.16 and 7.43–59.89, respectively. One can notice that both the estimates of the wall shear stress and the percentage of increase in the wall shear stress of the two-fluid Casson model are significantly lower than those of the two-fluid Herschel-Bulkley model.

Estimates of the resistance to flow (Λ) and the percentage of increase in the resistance to flow for the two-fluid Casson model and two-fluid Herschel-Bulkley model with $n = 0.95$ for different stenosis heights with $\beta = 0.985$, $A = \alpha = \alpha_H = 0.5$, $\theta = 0.1$, and $t = 45^\circ$ are given in Table 2. It is observed that, for the range 0.025–0.15 of the stenosis height, the corresponding

Table 2: Estimates of the resistance and percentage of increase in the resistance to flow (Λ) of the two-fluid Casson model and two-fluid Herschel-Bulkley model over uniform diameter tube for different stenosis heights with $A = \alpha = \alpha_H = 0.5$, $\beta = 0.985$, $\theta = 0.1$, and $t = 45^\circ$.

Stenosis height δ_p	Estimates of the resistance		Estimates of the percentage of increase in resistance	
	Two-fluid Casson model	Two-fluid H-B model with $n = 0.95$	Two-fluid Casson model	Two-fluid H-B model with $n = 0.95$
0.025	2.4795	2.9371	4.16	5.16
0.050	2.6135	3.0650	8.69	10.843
0.075	2.7616	3.2049	13.66	17.12
0.100	2.9258	3.3584	19.10	24.09
0.125	3.10868	3.5275	25.10	31.85
0.150	3.3131	3.7143	31.72	40.52

ranges of the percentage of increase in the estimates of the resistance to flow of the two-fluid Casson model and two-fluid Herschel-Bulkley model are 4.16–25.10 and 5.16–31.85, respectively. It is clear that both the estimates of the wall shear stress and the percentage of increase in the wall shear stress of the two-fluid Casson model are significantly lower than those of the two-fluid Herschel-Bulkley model. Hence, it is clear that the two-fluid Casson model layer is useful in the functioning of the diseased arterial system.

4. Conclusion

The pulsatile flow of blood through stenosed arteries is analyzed by assuming blood as a (i) two-fluid Casson model and (ii) two-fluid Herschel-Bulkley model. It is observed that, for a given set of values of the parameters, the velocity distribution of the two-fluid Casson model is considerably higher than that of the two-fluid Herschel-Bulkley fluid model. Further, it is noticed that the pressure drop, plug core radius, wall shear stress, and the resistance to flow of the two-fluid Casson model are significantly much lower than those of the two-fluid Herschel-Bulkley model.

It is of interest to note that the estimates of the wall shear stress and resistance to flow of the two-fluid Casson model are considerably lower than those of the two-fluid Herschel-Bulkley model. It is also worthy to note that the estimates of the percentage of increase in the wall shear stress and the percentage of increase in the resistance to flow of the two-fluid Casson model are considerably lower than those of the two-fluid Herschel-Bulkley model. Further, it is observed that the difference between the estimates of the wall shear stress, resistance to flow, percentage of increase in the estimates of the wall shear stress, and resistance to flow of the two-fluid Casson model and two-fluid Herschel-bulkley model is substantial. Hence, the two-fluid Casson model would be more useful in the mathematical analysis of the diseased arterial system.

References

[1] P. K. Mandal, "An unsteady analysis of non-Newtonian blood flow through tapered arteries with a stenosis," *International Journal of Non-Linear Mechanics*, vol. 40, no. 1, pp. 151–164, 2005.

[2] I. Marshall, S. Zhao, P. Papathanasopoulou, P. Hoskins, and X. Y. Xu, "MRI and CFD studies of pulsatile flow in healthy and stenosed carotid bifurcation models," *Journal of Biomechanics*, vol. 37, no. 5, pp. 679–687, 2004.

[3] D. S. Sankar and K. Hemalatha, "Pulsatile flow of Herschel-Bulkey fluid through stenosed arteries—a mathematical model," *International Journal of Non-Linear Mechanics*, vol. 41, no. 8, pp. 979–990, 2006.
[4] M. S. Moayeri and G. R. Zendehbudi, "Effects of elastic property of the wall on flow characteristics through arterial stenoses," *Journal of Biomechanics*, vol. 36, no. 4, pp. 525–535, 2003.
[5] S. Chakravarty and P. K. Mandal, "Two-dimensional blood flow through tapered arteries under stenotic conditions," *International Journal of Non-Linear Mechanics*, vol. 35, no. 5, pp. 779–793, 2000.
[6] G.-T. Liu, X.-J. Wang, B.-Q. Ai, and L.-G. Liu, "Numerical study of pulsating flow through a tapered artery with stenosis," *Chinese Journal of Physics*, vol. 42, no. 4, pp. 401–409, 2004.
[7] Q. Long, X. Y. Xu, K. V. Ramnarine, and P. Hoskins, "Numerical investigation of physiologically realistic pulsatile flow through arterial stenosis," *Journal of Biomechanics*, vol. 34, no. 10, pp. 1229–1242, 2001.
[8] R. K. Dash, G. Jayaraman, and K. N. Mehta, "Flow in a catheterized curved artery with stenosis," *Journal of Biomechanics*, vol. 32, no. 1, pp. 49–61, 1999.
[9] C. Tu and M. Deville, "Pulsatile flow of non-Newtonian fluids through arterial stenoses," *Journal of Biomechanics*, vol. 29, no. 7, pp. 899–908, 1996.
[10] S. Chien, "Hemorheology in clinical medicine," *Recent Advances in Cardiovascular Diseases*, vol. 2, pp. 21–26, 1981.
[11] V. P. Srivastava and M. Saxena, "Two-layered model of Casson fluid flow through stenotic blood vessels: applications to the cardiovascular system," *Journal of Biomechanics*, vol. 27, no. 7, pp. 921–928, 1994.
[12] P. Chaturani and R. P. Samy, "Pulsatile flow of Casson's fluid through stenosed arteries with applications to blood flow," *Biorheology*, vol. 23, no. 5, pp. 499–511, 1986.
[13] G. Bugliarello and J. Sevilla, "Velocity distribution and other characteristics of steady and pulsatile blood flow in fine glass tubes," *Biorheology*, vol. 7, no. 2, pp. 85–107, 1970.
[14] G. R. Cokelet, *The Rheology of Human Blood*, Prentice-Hall, Englewood Cliffs, NJ, USA, 1972.
[15] J. N. Kapur, *Mathematical Models in Biology and Medicine*, Affiliated East West Press, New Delhi, India, 1992.
[16] N. Iida, "Influence of plasma layer on steady blood flow in micro vessels," *Japanese Journal of Applied Physics*, vol. 17, no. 1, pp. 203–214, 1978.
[17] G. W. Scott-Blair, "An equation for the flow of blood, plasma and serum through glass capillaries," *Nature*, vol. 183, no. 4661, pp. 613–614, 1959.
[18] A. L. Copley, "Apparent viscosity and wall adherence of blood systems," in *Flow Properties of Blood and Other Biological Systems*, A. L. Copley and G. Stainsby, Eds., Pergamon Press, Oxford, UK, 1960.
[19] E. W. Merrill, A. M. Benis, E. R. Gilliland, T. K. Sherwood, and E. W. Salzman, "Pressure-flow relations of human blood in hollow fibers at low flow rates," *Journal of Applied Physiology*, vol. 20, no. 5, pp. 954–967, 1965.
[20] D. S. Sankar and U. Lee, "Two-phase non-linear model for the flow through stenosed blood vessels," *Journal of Mechanical Science and Technology*, vol. 21, no. 4, pp. 678–689, 2007.
[21] J. B. Shukla, R. S. Parihar, and S. P. Gupta, "Effects of peripheral layer viscosity on blood flow through the artery with mild stenosis," *Bulletin of Mathematical Biology*, vol. 42, no. 6, pp. 797–805, 1980.
[22] T. Karino and H. L. Goldsmith, "Flow behavior of blood cells and rigid spheres in annular vortex," *Philosophical Transactions of the Royal Society of London. Series B*, vol. 279, no. 967, pp. 413–445, 1977.